Contiguous-Channel Dual-Band Balanced Diplexer

Roberto Gómez-García[®], Senior Member, IEEE, José-María Muñoz-Ferreras[®], Member, IEEE, Li Yang[®], Member, IEEE, and Dimitra Psychogiou[®], Member, IEEE

Abstract—A class of balanced dual-band planar diplexer with frequency-contiguous channels for the differential mode and high common-mode rejection is presented. It exploits double-stub-loaded filtering cells with resistors connected at the symmetry plane of the overall diplexer. In this manner, a sharp-rejection dual-band operation for each diplexer channel with transmission zeroes (TZs) at both sides of the differential-mode dual passbands is obtained. In addition, broadened common-mode suppression and low common-mode in-band input power reflection can be realized. The theoretical foundations and design guidelines for the devised dual-band differential-mode diplexer are provided. Moreover, for practical-validation purposes, a microstrip prototype with imbricated 1.51-GHz/2.41-GHz and 1.92-GHz/2.85-GHz lower and upper dual-band channels is manufactured and tested.

Index Terms—Balanced diplexer, balanced filter, commonmode suppression, differential-mode diplexer, differential-mode filter, dual-band diplexer, microstrip diplexer, planar diplexer.

I. INTRODUCTION

WITH the advent of multiservice wireless communications and multimode radar systems, the development of frequency channelizers, multiplexers, and multiband bandpass filters (BPFs) is attracting a lot of attention. Balanced-/differential-mode operation is also desired for these RF devices as they show higher robustness to electromagnetic interference and common-mode noise. Thus, a variety of balanced multiplexers and multiband BPFs have been reported in the last few years based on different RF design approaches [1]–[9]. Out of them, only the ones in [8] and [9] correspond to diplexers with balanced-to-balanced operation and dual-band channels. However, their dual-band channels in differential-mode operation are not spectrally adjacent so that they are not suited for frequency-contiguous channelization applications.

In this letter, a class of balanced diplexer with imbricated/frequency-contiguous differential-mode dual-band channels is reported for the first time. It features: 1) differential-mode sharp-rejection passbands isolated by out-of-band transmission zeroes (TZs); 2) enlarged common-mode suppression bandwidth; and 3) low in-band common-mode input power reflection due to its common-mode input

Manuscript received January 5, 2019; revised February 14, 2019; accepted March 8, 2019. This work was supported in part by the Spanish Ministry of Economy, Industry, and Competitiveness (State Research Agency) under Project TEC2017-82398-R and in part by the National Science Foundation under Award 1731956. (Corresponding author: Roberto Gómez-García.)

- R. Gómez-García, J.-M. Muñoz-Ferreras, and L. Yang are with the Department of Signal Theory and Communications, University of Alcalá, Polytechnic School, 28871 Alcalá de Henares, Spain (e-mail: roberto.gomez.garcia@ieee.org; jm.munoz@uah.es; li.yang@uah.es).
- D. Psychogiou is with the Department of Electrical, Computer, and Energy Engineering, University of Colorado at Boulder, Boulder, CO 80309 USA (e-mail: dimitra.psychogiou@colorado.edu).

Color versions of one or more of the figures in this paper are available online at http://ieeexplore.ieee.org.

Digital Object Identifier 10.1109/LMWC.2019.2904396

quasi-absorptive behavior. Its RF operational and theoretical design principles are detailed in Section II. Furthermore, a proof-of-concept 1.51-GHz/1.92-GHz/2.41-GHz/2.85-GHz prototype is developed in microstrip technology and characterized in Section III.

II. THEORETICAL FOUNDATIONS

The circuit detail of the proposed dual-band balanced diplexer—symmetrical half part of the third-order architecture—is shown in Fig. 1(a). It consists of the combination of two balanced dual-band BPFs based on the in-series cascade connection of double-stub-loaded filtering cells and input/output power-matching sections. Fig. 1(b) depicts this double-stub-loaded filtering cell and its conceptual differential-and common-mode transfer functions. In differential-mode operation, it exhibits a one-pole dual-passband filtering response with center frequencies at f_{c1} and f_{c2} and TZs at 0, f_{z1} , and f_{z2} . In common-mode operation, the ending of one of the stubs with a physical ground and the other one with a loading resistor that is grounded at its other extreme allows to realize an enlarged common-mode suppression bandwidth.

A. Differential-Mode Analysis

Under differential-mode excitation, the connecting points of the balanced dual-band diplexer shown in Fig. 1(a) at the symmetry plane become virtual grounds. In this manner, a dual-band BPF action with TZs at both sides of the dual passbands is created by its resulting double-short-ended-stub-loaded cell as shown in Fig. 1(b). In particular, for design flexibility purposes so that the TZs at f_{z1} and f_{z2} are, respectively, generated by the stubs 1 and 2 within the spectral range $[0, f_{z2}]$ [see Fig. 1(b)], the following design conditions must be satisfied:

$$\frac{\pi}{2} \le \theta_2(f_{z1}) < \theta_1(f_{z1}) = \pi \tag{1}$$

$$\rightarrow 0 < f_{z1} < f_{z2} = \frac{\pi f_{z1}}{\theta_2(f_{z1})} \le 2f_{z1}. \tag{2}$$

At the center frequencies of the first and second dual passbands of the transfer function of the double-short-ended-stub-loaded cell f_{c1} (0 < f_{c1} < f_{c1}) and f_{c2} (f_{c1} < f_{c2} < f_{c2}), respectively, the input admittances of its stubs mutually cancel—i.e., $Y_1(f) + Y_2(f) = 0$ at $f = f_{c1}$, f_{c2} . This results, with (1) and (2), in the following condition to be met at $f = f_{c1}$, f_{c2} :

$$\tan\left[\left(\frac{\pi}{f_{z2}/f_{z1}}\right)\left(\frac{f}{f_{z1}}\right)\right] = -\frac{Z_1}{Z_2}\tan\left[\pi\left(\frac{f}{f_{z1}}\right)\right]. \quad (3)$$

By numerically solving (3), normalized-to- f_{z1} design curves for f_{c1} and f_{c2} as a function of Z_1/Z_2 and with f_{z2}/f_{z1} as a parameter can be derived. They are plotted in Fig. 2 for

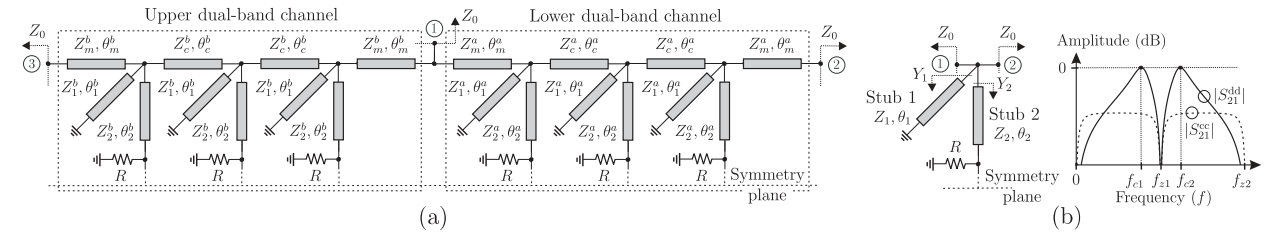


Fig. 1. (a) Proposed balanced dual-band diplexer (symmetrical half part for third-order realization). Z_0 : reference impedance. Z: characteristic impedances. θ : electrical lengths. R: resistance. (b) Constituent double-stub-loaded filtering cell with resistor (symmetrical half part) and conceptual differential-mode ($|S_{21}^{\rm cd}|$) and common-mode ($|S_{21}^{\rm cc}|$) power transmission responses. f_{c1} and f_{c2} : center frequencies of the differential-mode dual passbands. 0, f_{z1} , and f_{z2} : differential-mode TZ frequencies within the spectral range [0, f_{z2}]. Y_1 and Y_2 : input admittances of stubs 1 and 2.

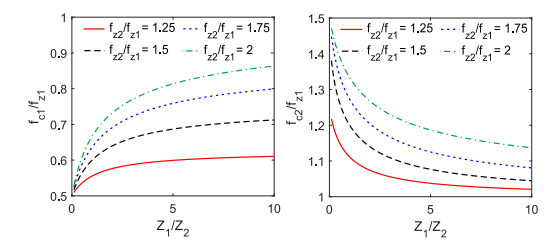


Fig. 2. Normalized-to- f_{z1} theoretical design curves for f_{c1} and f_{c2} as a function of Z_1/Z_2 and with f_{z2}/f_{z1} as a parameter.

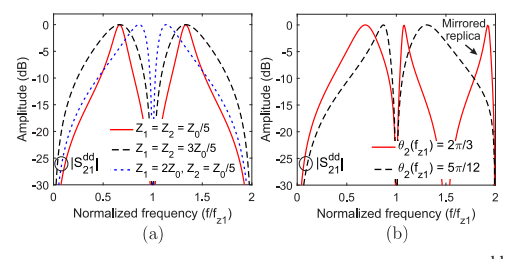


Fig. 3. Theoretical synthesized power transmission responses ($|S_2^{\rm dd}|$) with the resulting double-short-ended-stub-loaded cell in Fig. 1(b) for the differential mode with the design curves in Fig. 2 and (1) and (2). (a) Symmetrical response examples $[\theta_1(f_{z1}) = \pi$ and $\theta_2(f_{z1}) = \pi/2]$. (b) Asymmetrical response examples $[Z_1 = 3Z_0/5, Z_2 = Z_0/5, \text{ and } \theta_1(f_{z1}) = \pi]$.

 $f_{z2}/f_{z1} = 1.25, 1.5, 1.75$, and 2. Note that the line-impedance degree of freedom in Z_1/Z_2 can be used to simultaneously adjust the values of the two dual-band bandwidths, whereas their independent control requires to also act on f_{z1} and f_{z2} .

Illustrative examples of theoretical synthesized responses—with the design curves in Fig. 2 and (1) and (2)—of the resulting double-short-ended-stub-loaded cell in Fig. 1(b) for the differential mode are shown in Fig. 3. As can be seen, a full control of the dual-band center frequencies and bandwidths is feasible. Note that a case for which $\theta_2(f_{z1}) < \pi/2$ so that $f_{z2} = 2f_{z1}$ —now generated by stub 1—is also shown, which results in a broader bandwidth for the upper dual passband.

B. Common-Mode Analysis

Under common-mode excitation, one of the stubs—stub 1—of the double-stub-loaded filtering cell shown in Fig. 1(b) remains ended in a physical ground, and the other one—stub 2—is terminated in a grounded resistor. In this manner, the common-mode rejection bandwidth can be maximized with regard to the case of not including this resistor—i.e., stub 2 ended in a virtual open circuit for the common mode—as proven in the following.

1) For a specific differential-mode dual-band response that is shared by all the cases shown in Fig. 4(a) of the double-stub-loaded filtering cell, this figure shows the effect on its common-mode response of

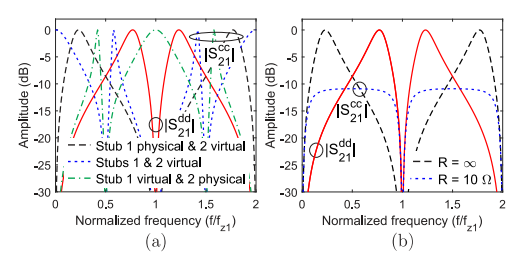


Fig. 4. (a) Effect of the terminations of the stubs—i.e., physical or virtual grounds—of the double-stub-loaded filtering cell on the common-mode power transmission response $(|S_{21}^{cc}|)$ for $R=\infty$. (b) Effect of R on the common-mode power transmission response $(|S_{21}^{cc}|)$ of the double-stub-loaded filtering cell with the stub terminations in Fig. 1(b). For all represented responses, $Z_1=3Z_0/5$, $Z_2=Z_0/5$, $\theta_1(f_{z1})=\pi$, and $\theta_2(f_{z1})=\pi/2$.

selecting the termination of its two stubs as physical or virtual—i.e., connection at the edge at the symmetry plane—grounds. As observed, the adopted choice—i.e., stub 1 ended in a physical ground and stub 2 connected at the symmetry plane at its extreme as shown in Fig. 1(b)—is the optimum one in terms of common-mode suppression levels within the differential passbands.

2) For the differential-mode two-band response in Fig. 4(a) and the scheme in Fig. 1(b), Fig. 4(b) analyzes the resistor effect. As shown, it allows to enlarge the common-mode suppression bandwidth—as needed in this balanced diplexer application so that it covers all its bands—but at the expense of decreased common-mode power-rejection levels throughout the differential-mode dual passbands.

III. EXPERIMENTAL RESULTS

To validate the practical viability of the proposed balanced dual-band diplexer principle, a 50-Ω microstrip prototype with third-order dual-band channels has been manufactured and tested. It was ideally designed so that the differential-mode passbands of the dual-band channels are imbricated. They exhibit center frequencies of 1.49 and 2.4 GHz—lower dual-band channel or first/third diplexer bands—and center frequencies of 1.91 and 2.86 GHz—upper dual-band channel or second/fourth diplexer bands. In both dual-band channels, the 3-dB absolute bandwidths of the lower and upper differential-mode passbands are about 400 and 365 MHz.

The theoretical diplexer design was done with the design rules and curves previously given followed by an optimization of the entire circuit. The theoretical differential- and common-mode S-parameters in the amplitude of this diplexer are shown in Fig. 5. As shown, sharp-rejection dual-band differential-mode channels with input power-matching levels above 15 dB and a minimum 11.3-dB output power-isolation

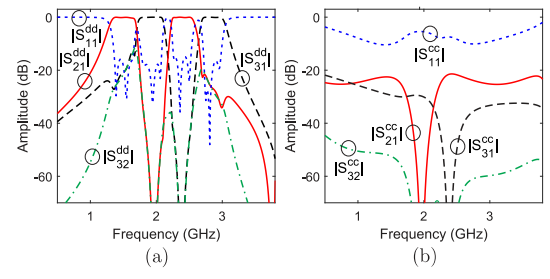


Fig. 5. Theoretical differential- and common-mode S-parameters of the designed balanced dual-band diplexer ($f_{z1}^a=1.97~\mathrm{GHz}, f_{z1}^b=2.38~\mathrm{GHz},$ and $Z_0=50~\Omega$; lower dual-band channel—Fig. 1(a): $Z_1^a=2.04Z_0, Z_2^a=Z_0, Z_c^a=2.4Z_0, Z_m^a=1.58Z_0, \theta_1^a(f_{z1}^a)=\pi, \theta_2^a(f_{z1}^a)=0.523\pi, \theta_c^a(f_{z1}^a)=0.492\pi,$ and $\theta_m^a(f_{z1}^a)=0.492\pi$; upper dual-band channel—Fig. 1(a): $Z_1^b=2.74Z_0, Z_2^b=0.8Z_0, Z_c^b=2.76Z_0, Z_m^b=1.58Z_0, \theta_1^b(f_{z1}^b)=\pi, \theta_2^b(f_{z1}^b)=0.521\pi, \theta_c^b(f_{z1}^b)=0.44\pi,$ and $\theta_m^b(f_{z1}^b)=0.463\pi$). (a) Differential-mode power transmission ($|S_{21}^{\rm cd}|$ and $|S_{31}^{\rm cd}|$), output power-isolation ($|S_{32}^{\rm cd}|$), and input power-reflection ($|S_{11}^{\rm cd}|$) parameters. (b) Common-mode power transmission ($|S_{21}^{\rm cd}|$ and $|S_{31}^{\rm cd}|$), output power-isolation ($|S_{32}^{\rm cc}|$), and input power-reflection ($|S_{11}^{\rm cd}|$) parameters.

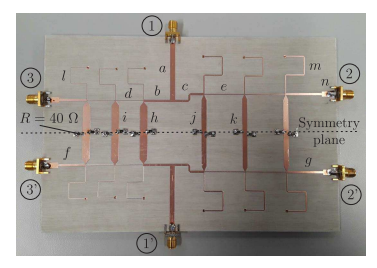


Fig. 6. Photograph of the manufactured microstrip prototype of balanced dual-band diplexer (Rogers 4003C substrate: relative dielectric permittivity $\varepsilon_r=3.38$, dielectric thickness H=1.524 mm, metal thickness $t=35~\mu\text{m}$, and dielectric loss tangent $\tan(\delta_D)=0.0027$; ground connections for $40\text{-}\Omega$ resistors and short-ended stubs: 1-mm-diameter metallic via holes; nonredundant dimensions of one symmetrical circuit half in mm—"w" stands for width and "l" for length: $w_a=3.48$, $l_a=41.4$, $w_b=1.5$, $l_b=17$, $w_c=1.5$, $l_c=21.1$, $w_d=0.3$, $l_d=18$, $w_e=0.5$, $l_e=26$, $w_f=1.5$, $l_f=17$, $w_g=1.5$, $l_g=23$, $w_h=4.9$, $l_h=15.5$, $w_i=4.9$, $l_i=16.1$, $w_j=3.5$, $l_j=20$, $w_k=3.5$, $l_k=20.5$, $w_l=0.3$, $l_l=40.6$, $w_m=0.8$, $l_m=47.3$, $w_n=3.48$, $l_n=10$, and taper length: 3 mm).

level—overlapping region between the first/second diplexer channels—within their 3-dB bandwidths are obtained. An input common-mode quasi-absorptive behavior due to the resistors is also observed.

A photograph of the built prototype of balanced diplexer is shown in Fig. 6. Its simulated and measured differential- and common-mode S-parameters in amplitude and group delay curves are compared in Fig. 7, showing a fairly close agreement. The main measured characteristics of this dual-band balanced diplexer prototype are as follows. Lower dual-band channel—first/third differential-mode diplexer bands: center frequencies of 1.51 and 2.41 GHz, 3-dB absolute bandwidths equal to 414 and 343 MHz, minimum in-band power-insertion-loss levels of 0.55 and 1.09 dB, minimum in-band input power-matching levels of 14.55 and 11.55 dB, and maximum in-band group delay variations of 3.5 and 3.9 ns. Upper dual-band channelsecond/fourth differential-mode diplexer bands: center frequencies of 1.92 and 2.85 GHz, 3-dB absolute bandwidths equal to 387 and 333 MHz, minimum in-band powerinsertion-loss levels of 0.86 and 1.36 dB, minimum in-band input power-matching levels of 13.95 and 15.2 dB, and maximum in-band group delay variations of 2.4 and 1.8 ns. The minimum common-mode attenuation level within the 3-dB bandwidths of the differential-mode passbands is 19.4 dB.

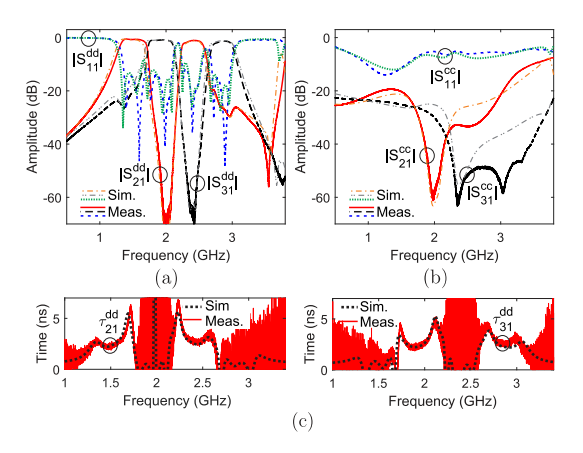


Fig. 7. Simulated (with Ansys HFSS) and measured differential- and common-mode S-parameters of the microstrip prototype of balanced dual-band diplexer. (a) Differential-mode power transmission ($|S_{21}^{\rm cd}|$ and $|S_{31}^{\rm dd}|$) and input power reflection ($|S_{11}^{\rm cd}|$) parameters. (b) Common-mode power transmission ($|S_{21}^{\rm cc}|$ and $|S_{31}^{\rm cc}|$) and input power-reflection ($|S_{11}^{\rm cc}|$) parameters. (c) Differential-mode transmission group delay ($\tau_{21}^{\rm dd}$ and $\tau_{31}^{\rm dd}$) responses.

IV. CONCLUSION

A type of differential-mode dual-band diplexer has been presented. This diplexer, which avoids the use of coupled-line sections and reactive lumped elements, features: 1) imbricated/frequency-contiguous differential-mode dual passbands that are isolated through TZs in each channelizing filter; 2) broadband common-mode suppression; and 3) common-mode low in-band input power reflection. Its theoretical foundations and design rules have been given, and a proof-of-concept microstrip prototype has been built and measured.

REFERENCES

- J. Shi and Q. Xue, "Dual-band and wide-stopband single-band balanced bandpass filters with high selectivity and common-mode suppression," *IEEE Trans. Microw. Theory Techn.*, vol. 58, no. 8, pp. 2204–2212, Aug. 2010.
- [2] F. Wei, Y. J. Guo, P.-Y. Qin, and X. W. Shi, "Compact balanced dualand tri-band bandpass filters based on stub loaded resonators," *IEEE Microw. Wireless Compon. Lett.*, vol. 25, no. 2, pp. 76–78, Feb. 2015.
- [3] S.-X. Zhang, L.-L. Qiu, and Q.-X. Chu, "Multiband balanced filters with controllable bandwidths based on slotline coupling feed," *IEEE Microw. Wireless Compon. Lett.*, vol. 27, no. 11, pp. 974–976, Nov. 2017.
- [4] R. Gómez-García, J.-M. Muñoz-Ferreras, W. Feng, and D. Psychogiou, "Balanced symmetrical quasi-reflectionless single-and dual-band bandpass planar filters," *IEEE Microw. Wireless Compon. Lett.*, vol. 28, no. 9, pp. 798–800, Sep. 2018.
- [5] Y. Zhou, H.-W. Deng, and Y. Zhao, "Compact balanced-to-balanced microstrip diplexer with high isolation and common-mode suppression," *IEEE Microw. Wireless Compon. Lett.*, vol. 24, no. 3, pp. 143–145, Mar. 2017.
- [6] X. Guo, L. Zhu, and W. Wu, "Balanced diplexers based on inner-coupled dual-mode structures with intrinsic common-mode suppression," *IEEE Access*, vol. 5, pp. 26774–26782, 2017.
- [7] A. Fernández-Prieto, A. Lujambio, F. Martín, J. Martel, F. Medina, and R. R. Boix, "Compact balanced-to-balanced diplexer based on split-ring resonators balanced bandpass filters," *IEEE Microw. Wireless Compon. Lett.*, vol. 28, no. 3, pp. 218–220, Mar. 2018.
- [8] W. Jiang, Y. Huang, T. Wang, Y. Peng, and G. Wang, "Microstrip balanced quad-channel diplexer using dual-open/short-stub loaded resonator," in *IEEE MTT-S Int. Microw. Symp. Dig.*, San Francisco, CA, USA, May 2016, pp. 1–3.
- [9] C.-H. Lee, C.-I. G. Hsu, S.-X. Wu, and P.-H. Wen, "Balanced quad-band diplexer with wide common-mode suppression and high differentialmode isolation," *IET Microw., Antennas Propag.*, vol. 10, no. 6, pp. 599–603, Apr. 2016.